Available online at www.sciencedirect.com

ScienceDirect

Procedia Structural Integrity 28 (2020) 538–545

Structural Integrity Procedia

www.elsevier.com/locate/procedia

1st Virtual European Conference on Fracture

Fiber push-in failure in carbon fiber epoxy composites

Andreas J. Brunner[a]*, Johann J. Schwiedrzik[b], Gaurav Mohanty[b,c], Johann Michler[b]

[a]*Empa, Swiss Federal Laboratories for Materials Science and Technology, Laboratory for Mechanical Systems Engineering, Überlandstrasse 129, CH-8600 Dübendorf, Switzerland*

[b]*Empa, Swiss Federal Laboratories for Materials Science and Technology, Laboratory for Mechanics of Materials & Nanostructures, Feuerwerkerstrasse 39, CH-3602 Switzerland*

[c]*Materials Science and Environmental Engineering, Tampere University, FI-33014 Tampere, Finland*

Abstract

Micromechanical quasi-static and cyclic fiber push-in tests performed with an indenter in-situ in a scanning electron microscope on polished slices (thickness around 300 μm) of carbon-fiber epoxy composites provide information on the effect of fiber density on the fiber-matrix debonding and the fiber failure. Specifically, "close-packed", i.e., fibers surrounded by six nearest neighbor fibers (called "hexagonal" hereafter) versus "isolated" fibers, defined as fibers at least one fiber diameter distant from the next nearest fiber, were compared. In spite of the more compliant behavior of isolated fibers under quasi-static and cyclic indentation loads, initiation of fiber-matrix debonding and push-in failure (fiber splitting into two or three parts) occurred at roughly comparable loads for both, "hexagonal" and "isolated" fibers. Earlier tests on thinner slices of such composites (thickness around 30 μm) had resulted in full debonding and fiber push-out without fiber failure. The fibers in the thicker slices showed first indenter imprints on the surface and an increasing hysteretic behavior in the load-displacement curves before debonding. The analysis of the cyclic load-displacement curves yields the elastic-plastic and the hysteretic (debonding) energy contributions.

Keywords: fiber-reinforced polymer-matrix composites: carbon fiber: epoxy matrix; fiber push-in; in-situ scanning electron microscopy;

* Corresponding author. Tel.: +41-58-765-4493; fax: +41-58-765-6911.
E-mail address: andreas.brunner@empa.ch

10.1016/j.prostr.2020.10.063

1. Introduction

Carbon fiber-reinforced polymer (CFRP) composites with epoxy matrix have found use in various structural, usually load-bearing applications or in structural repair and their usage is expected to increase further, see, e.g., Hollaway (2010) or Jölly et al. (2015). CFRP epoxy laminates, however, suffer from inherently weak matrix dominated properties, notably limited delamination and shear resistance as discussed, e.g., by Brunner et al. (2008) and Sharma et al. (2014). One approach for improving these properties aims at designing matrix-fiber interphases that yield higher interfacial adhesion or toughness in order to prevent initiation of debonding or shear failure, see, e.g., Bekyarova et al. (2007) and Yao et al. (2015).

There are several micromechanical tests for characterizing interfacial adhesion or interfacial shear strength described and discussed in literature. Early publications (Herrera-Franco and Drzal 1992) discuss the micro-bond test (using a fiber with a micro-droplet of resin), the single-fiber fragmentation test (SFFT, with a single fiber embedded in a so-called "dogbone"-shaped matrix), and the micro-debond/micro-indentation test. Teklal et al. (2018) review the available micromechanical tests for characterizing fiber-matrix adhesion. The tests reviewed comprise fiber indentation, fiber fragmentation, fiber pull-out and compression. This property is important for the macroscopically determined interlaminar shear strength (ILSS). Stojcevski et al. (2019) discuss interfacial shear strength (IFSS) tests on different scales from the micro- to the macro-level and compare these. The respective micromechanical test is the SFFT. An alternative Multi-Fiber Fragmentation Test (MFFT) for determining IFFS was recently presented by McCarthy and Soutis (2019).

Various approaches for improving the interfacial adhesion between fiber and matrix or the IFSS have been discussed in literature, see, e.g., Drescher et al. (2013), Sharma et al. (2014), Karger-Kocsis et al. (2015), Yuan et al. (2019), or Kumar et al. (2020). Beside various surface treatments of the carbon fibers, e.g., acid oxidation, sizing coating, silane coupling, discussed for example by Yuan et al. (2019), the deposition of carbon based or other nano- and micron-scale particles for creating hierarchically structured fiber surfaces or interfaces are also reported in literature: Among them are graphene oxide (GO) particles (Awan et al. 2019, Yuan et al. 2019), carbon nanotubes (CNT) of different types (Ashrafi et al. 2011, Awan et al. 2018), possibly functionalized with different chemical groups, silica nano- or micro-spheres (Zhang et al. 2013), or combinations of such particles. Kinloch et al. (2018) recently critically examined the interactions between epoxy (matrix material) and GO or CNT in epoxy-based nanocomposites. These interactions would also be relevant for fiber-matrix interphase engineering in the respective hierarchical fiber epoxy-composites.

Nomenclature

CFRP	Carbon Fiber-Reinforced Polymer
CNT	Carbon Nano-Tube(s)
EPD	Electro-Phoretic Deposition
FEM	Finite Element Model(ling)
GO	Graphene Oxide
IFSS	Interfacial Shear Strength
ILSS	Interlaminar Shear Strength
MFFT	Multifiber Fragmentation Test
SEM	Scanning Electron Microscope
SFFT	Single Fiber Fragmentation Test

Decorating the carbon fibers with multi-walled CNT via an electro-phoretic deposition (EPD) process by Battisti et al. 2014) or Kim et al. (2015) has indicated some improvement in fiber-matrix adhesion or in (macroscopic) ILSS as well as simultaneously improved fiber push-out behavior in quasi-static micro-mechanical single fiber push-out testing. Finite Element Modelling (FEM) of single fiber push-out by Rodriguez et al. (2012) and Esqué-de los Ojos et al. (2016) has provided indications of the relevant parameters for this behavior. The present contribution extends these efforts to cyclic single fiber push-in analogous to the approach developed for ceramic fibers by Mueller et al. (2015)

and later applied to CFRP with thermoplastic polymer matrix by Greisel et al. (2014) and by Jäger et al. (2015) for CFRP with thermoset (epoxy) matrix. The current presentation also includes consideration of the effects of the local fiber environment, i.e., close packed "hexagonal" fibers compared with single "isolated" fibers (the latter are defined as fibers at least one fiber diameter away from the nearest neighboring fiber).

2. Materials and Methods

Unidirectional laminates were manufactured from unsized carbon fibers (type AS4 from Hexcel) with an epoxy matrix (resin type Araldite® LY564 with amine-type hardener XB 3486 from Huntsman, resin-hardener ratio 100:34, mixed for about 10 minutes at 500 rpm in a high-speed shear mixer) with a vacuum-assisted resin-infusion process (at 50 mbar, duration around 25 minutes). The laminates were then cured at +50°C for 15 hours at a pressure of 50 bar and let cool to ambient temperature by switching the furnace off.

In a first step, specimens with a size of 85 mm x 10 mm were machined from the laminate (thickness around 1.55 mm). The single fiber push-in specimens were then prepared from these beams by cutting a slice of roughly 1mm thickness off (cross-section of 10 mm x 1.55 mm). Grinding and polishing the slices was performed by mounting them on a grinder (type Fischione Model 160) and polishing on an equipment (type Phoenix 4000 from Bühler) with paper and cloth, respectively, of increasingly finer grit to obtain parallel, smooth faces and slices of a thickness around 300 μm.

These slices were then mounted on standard scanning electron microscope (SEM) sample holders using a thermoplastic adhesive (type crystalbond™). The push-in experiments were per-formed with a displacement controlled Alemnis indenter described by Ghisleni et al. (2009) and Mohanty et al. (2015) within the chamber of a SEM (type DSM962 from Zeiss). The indenter tip used was a custom-made diamond pillar with 4 μm diameter and a height of 6 μm, obtained by focused ion beam milling of a flat punch diamond indenter. Fibers for push-in were selected among those showing hexagonal close packing of neighboring fibers as well as “isolated” fibers at least one fiber diameter (around 6-7 μm) away from the nearest neighbor. Two types of push-in experiments were performed analogous to those described by Battisti et al. (2014), i.e., (a) quasi-static loading with a loading/unloading rate of 100 nm/s and an imposed maximum displacement of 10 μm and (b) cyclic loading with constant loading/unloading rate of 100 nm/s, with a first cycle composed of a 2 μm displacement, starting at an indenter tip position about 2 μm ±50nm above the fiber. The displacement was then incremented in steps of 200 nm for each cycle (followed by complete unloading) until a maximum displacement of 10 μm. SEM still images were taken before and after the tests and the push-in process recorded by a video camera in the SEM chamber.

The non-linear and maximum load-points, the corresponding displacements and the remaining plastic deformation after unloading (on the time-scale of minutes for these test) as well as the slope of the load-displacement plots in the linear range, and the different energy contributions were determined from the data recorded by the indenter equipment for the first ten cycles of each test by a MATLAB routine developed by one of the authors (J.J.S.).

3. Results and Discussions

Fig. 1 (left) shows a comparison of the load-displacement curves of two "hexagonal" fibers recorded with the Alemnis indenter. One curve (shown in blue) is from a quasi-static push-in test, the other (shown in red) the envelope of a cyclic indentation test. Please see Fig. 2 (right) for the full load-displacement curve from the cyclic push-in test for comparison. The agreement between the envelope of the cyclic test and the quasi-static curve is very good. Both curves show almost the same initial slope (indicating comparable stiffness of the local fiber environment) and almost the same load at the non-linear point of the load-displacement curve. Even the first maximum loads of both curves are similar. However, beyond that point the two curves differ. In the curve from the quasi-static test, the load drops by roughly 20 mN (about 20% of the peak load), whereas the load of the cyclic test levels off and then continues with a slight increase with additional cycles. A further difference between the two curves is that above the non-linear load point the envelope of the cyclic load curve shows a slightly steeper slope, i.e., reaches the first maximum load at lower displacement. Fig. 1 (right) shows an image taken inside the SEM equipment with the indenter tip above a "hexagonal" fiber. This image was taken after ten load cycles, i.e., before the maximum load was reached. In spite of the limited quality and resolution of the video image, the top of the fiber shows a clear indentation mark caused by the previous

load cycles. However, after ten load cycles no clear indication of either debonding from the matrix surrounding the fiber nor of incipient fiber failure is observed in the video image. Fig. 2 (left) shows the load-displacement curve for load cycle number twelve, i.e., the cycle during which the fiber failed. Figure 2 (right) shows the respective SEM video image after the completion of this cycle. The fiber essentially is split along the horizontal axis in the image. Whether there is third crack in the fiber surface orthogonal to the "horizontal" crack cannot be clearly seen (due to the limited quality of the video image). The load-displacement curve of cycle number twelve indicates some plastic deformation. The load increase starts at a displacement of about 170 nm and upon unloading reaches a value of 0 mN at about 380 nm displacement. This indicates that the indenter imprint caused by the preceding eleven load steps amounted to less than 200 nm. The load increase shows a (slight) non-linear point around 20 mN, but then continues again in a fairly linear manner with lower slope up to about 90 mN. Very likely, this latter load level corresponds to the failure of the fiber, followed by a rather "soft" push-in that requires little additional load increase (i.e., the roughly constant load observed at increasing displacement).

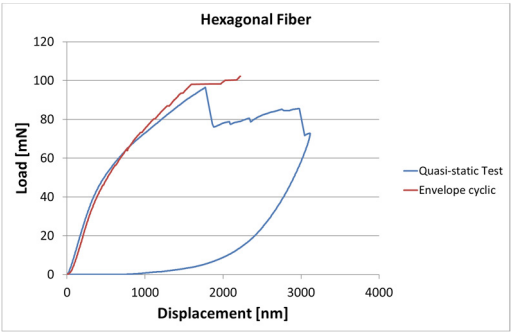

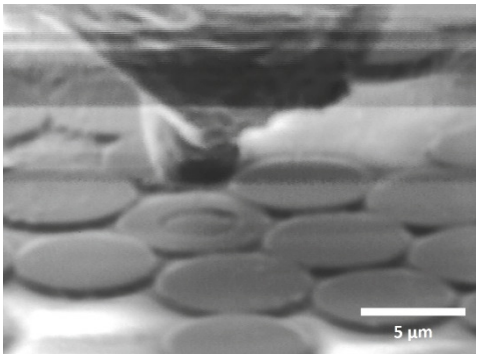

Fig. 1 (left) Comparison of the load-displacement curve from a quasi-static push-in test on a hexagonal fiber with the envelope of a cyclic push-in test; (right) SEM video image of a hexagonal fiber after 10 cycles (before maximum load and failure) showing an indentation mark on the top.

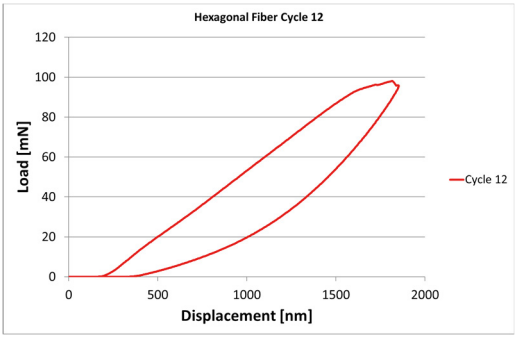

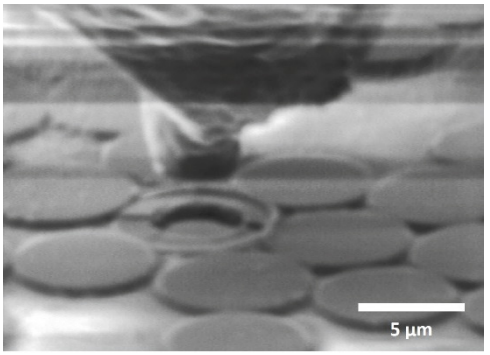

Fig. 2 (left) Load-displacement push-in curve for the cycle number 12 during which the "hexagonal" fiber failed (please note the change in displacement scale on the x-axis compared to other figures) and (right) SEM image of the fiber after failure.

Fig. 3 compares the cyclic load-displacement curves from fiber push-in for (left) an "isolated" and (right) a "hexagonal" fiber (both curves in blue) with the respective envelopes shown in red. Even though the initial slopes are different as noted above, the first non-linear load-point in both cases occurs around 40 mN with a scatter on the order of a few mN at most. Similar loads of the non-linear point (amounting to about 40-45 mN) have been observed in push-out tests performed on thinner slices of CFRP with epoxy matrix by Battisti et al. (2014). Intuitively, the non-linear load point may be thought of representing a first indication of failure, e.g., analogous to standard fracture toughness or delamination tests on FRP composites (see, e.g., Brunner et al. (2008) for a discussion). The detailed analysis of single fiber push-out tests on CFRP with thermoset epoxy matrix by Jäger et al. (2015), however, concludes that the cause is not crack opening, but plastic deformation of the matrix material. This is consistent with the evidence from the video imaging performed in the present investigation.

Clear differences between the different fiber-environment, however, are observed after fiber failure (see Fig. 3). The "isolated" fibers yield a significant drop in load as well as a reduction in the slope of the loading part of the curves in the following load cycles, whereas the peak loads hardly change for the "hexagonal" fibers. The slope of the loading part of the cycles after fiber failure are reduced less in the case of "hexagonal" fibers. It is interesting to note the difference between the quasi-static load-displacement curve for a hexagonal fiber shown in Fig. 1 and the respective curve for cyclic loading of another hexagonal fiber (envelope shown in Fig. 1, full curve in Fig. 3) with respect to the behavior after fiber failure.

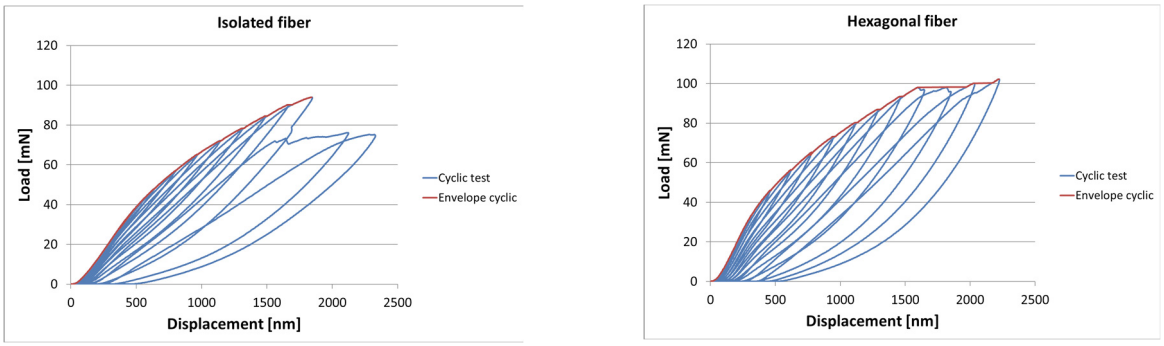

ig. 3 (left) Load-displacement push-in curve and envelope for "isolated" fiber for comparison with that (right) from a "hexagonal" fiber.

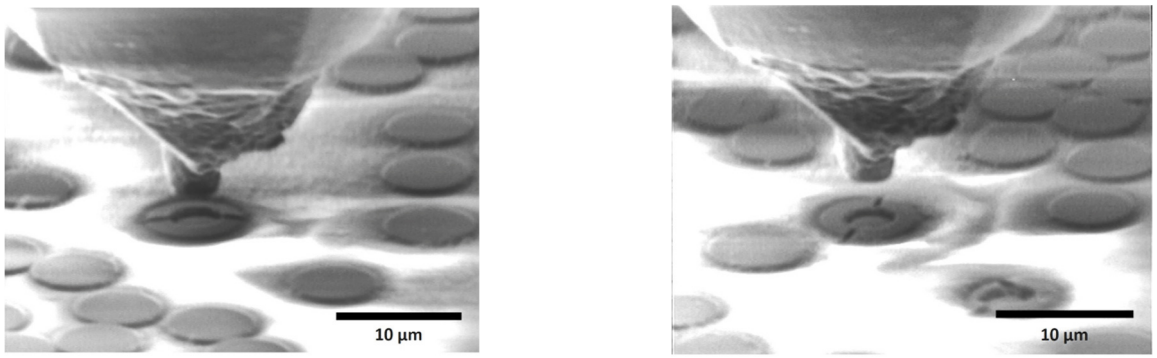

ig. 4 Comparison of an SEM video image of the failure of (left) an "isolated" fiber with that (right) and a fiber with at least one nearest neighbor, both after cyclic after push-in.

Fig. 4 shows a comparison between the failure of an isolated fiber (left) with that of a fiber with at least one nearest neighbor (right). Both video images in parts are affected by charging effects producing a slightly blurred image, but the individual fibers can still be recognized. However, at first sight it is difficult to clearly see whether the isolated fiber that has been tested (Fig. 4 left; indenter imprint on top) really debonded from the surrounding matrix. The isolated fiber under test shows the indenter imprint at the center and a horizontal splitting crack analogous to that shown in Fig. 2 (right) for a hexagonal fiber. Compared with other fibers not yet tested, very likely the whole fiber is debonded. This is deduced from the slight displacement of the top of the fiber relative to the matrix surrounding it. This differs from the image of other fibers that were not tested; these slightly protrude from the matrix. The hexagonal fiber shows the same indenter imprint and crack as the isolated fiber, but it is not the full fiber that is pushed into the matrix. A thin fiber "rim" still remains and it is not clear whether the fiber fully or only partially debonded from the surrounding matrix, or not at all. Whether this rather unusual type of failure is due to a fiber defect below the surface or superior fiber-matrix adhesion, or a combination of both, cannot be clearly determined from the video image.

Compared with the fiber push-out tests performed on "thin" slices of CFRP laminates with a thickness around 30 µm reported by Battisti et al. (2014), the "thick" slices (around 300 µm) all show fiber failure before full debonding and little overall push-in displacement after failure (less than 400-500 nm). This holds independent of whether

"isolated" or "hexagonal" fibers are tested. The implication is that the test set-up yields different failure behavior depending on the thickness of the slice. Since the debonded length and area of the fibers in the thicker slice cannot be determined in the push-in experiment, it is not possible to quantitatively calculate the adhesion toughness, contrary to the case of the thin slice with full debonding where the respective area is known. Nevertheless, it is expected that modified fiber-matrix interface may yield improved adhesion and interfacial toughness on the microscopic scale. This may result in improvements of the corresponding, macroscopic properties (IFSS, ILSS). The correlation between local fiber-matrix behavior (adhesion or toughness) with macroscopic defect formation and failure can, however, be complex. As shown by Battisti et al. (2014), the difference between unmodified fibers and those treated with CNT or after oxidation in push-out tests with thin slices only became significant, once the fiber fragments had fully debonded and started to be pushed out. This indicates that fiber surface modification may not always be effective in improving first adhesion failure, i.e., the initiation of debonding between fiber and matrix.

Table 1 shows the plastic and hysteretic energy contributions derived from the load cycles in the push in tests and compares values from an isolated fiber with those from a hexagonal fiber. The plastic energy contributions of both fibers are similar and increase with cycle number up to a factor between about 15 and 25 (comparing cycle 1 and cycle 10). However, in comparison with the hysteretic energy contribution, the values remain rather low (between about 200x and 400x10^{-12} J). The hysteretic energy contributions do increase significantly, by orders of magnitude (effectively, the factors derived from Table 1 between cycle 1 and cycle 10 are 76 and around 2000, respectively) and the values reach between 38000x and 46000x10^{-12} J. Of course, there is a fairly large scatter among the individual fibers, even if the same type (isolated or hexagonal) is considered, but the trends (data not shown) are similar to those shown here.

Table 1. Values of elastic-plastic and hysteretic energy contributions calculated from the individual cycles of the load-displacements curves for one isolated and one hexagonal fiber.

Cycle number	Plastic Energy [10^{-12} J] Isolated Fiber	Hysteretic Energy [10^{-12} J] Isolated Fiber	Plastic Energy [10^{-12} J] Hexagonal Fiber	Hysteretic Energy [10^{-12} J] Hexagonal Fiber
Cycle 1	12.3	498.0	7.0	22.4
Cycle 2	19.7	2564.9	11.7	1079.9
Cycle 3	23.5	6398.8	20.1	3947.9
Cycle 4	32.6	11783.8	33.7	8526.6
Cycle 5	41.8	18181.0	45.8	14217.8
Cycle 6	55.8	25030.5	65.4	20338.1
Cycle 7	71.3	32030.7	84.9	26627.6
Cycle 8	90.7	38870.2	109.4	33021.9
Cycle 9	117.5	45637.5	138.4	39320.4
Cycle 10	187.1	38000.4	168.0	45533.4

4. Conclusions and Ontlook

The results (non-linear and maximum load points around 40 mN and 100 mN, respectively) for single fiber push-in presented here for CFRP epoxy slices of about 300 μm thickness indicate that first damage (likely plastic deformation of the matrix) and failure in the adhesion between carbon fibers and epoxy matrix do not strongly depend on the local fiber density in the push-in tests. The local stiffness, however, quantified by the initial slope of the loading curves, differs and is higher for the closed-packed "hexagonal" fiber arrangement. For "thin" slices of around 30 μm, the respective values reported by Battisti et al. (2014) the non-linear loads for the equivalent material are about 40-45 mN, i.e., essentially comparable. However, the maximum loads are around 60 mN, i.e., clearly lower than those observed here. This is likely due to the fact that in the thin slices the fibers debond completely and then are pushed out, In thicker slices, the fibers only debond partially (not along the full length of the fiber-matrix interface as the fibers in the thin slices) and then fail under compressive stress. This mode of failure apparently requires higher loads

than push-out of fully debonded, sufficiently short fiber fragments where the main contribution is likely the friction between the fiber surface and the matrix. As discussed by Battisti et al. (2014), modification of the fiber surface, e.g., decoration with nanoparticles such as CNT or plasma treatment, both increasing the roughness of the fiber surface, tend to yield higher friction in push-out than untreated fiber surfaces.

The quasi-static and cyclic fiber push-out in sufficiently thin slices of CFRP laminates and the respective quasi-static and cyclic push-in failure in thicker slices provide information on the fiber-matrix adhesion, at least for the initiation of debonding. Quantification of interfacial toughness is, however, difficult from the fiber push-in tests, since the area of the debonded fiber-matrix interface cannot be quantified at the failure loads. The methodology presented here will be useful for qualitatively comparing different fiber-matrix interface treatments or differently engineered interphases.

Acknowledgements

Dr Dietmar Haba (Empa) is gratefully acknowledged for the specimen preparation and Prof. Markus G.R. Sause (Augsburg University) for discussion of push-in tests and analysis.

References

Ashrafi, B., Guan, J.W., Mirjalili, V., Zhang Y:F., Chun, L. Hubert, P., Simard, B., Kingston, C.T., Bourne, O., Johnston, A. 2011. Enhancement of mechanical performance of epoxy/carbon fiber laminate composites using single-walled carbon nanotubes. Composites Science and Technology 71, 1569–1578.

Awan, F.S., Fakhar, M.A., Khan, L.A., Zaheer, U., Khan, F.A., Subhani, T. 2018. Interfacial mechanical properties of carbon nanotube-deposited carbon fiber epoxy matrix hierarchical composites. Composite Interfaces 25(8), 681-699.

Awan, F.S., Fakhar, M.A., Khan, L.A., Subhani, T. 2019. Study of Interfacial Properties of Carbon Fiber Epoxy Matrix Composites Containing Graphene Nanoplatelets. Fibers and Polymers 20(3), 633-641.

Battisti, A., Esqué-de los Ojos, D., Ghisleni, R., Brunner, A.J., 2014. Single fiber push-out characterization of interfacial properties of hierarchical CNT-carbon fiber composites prepared by electrophoretic deposition. Composites Science and Technology 95, 121-127.

Bekyarova, E., Thostenson, E.T., Yu, A., Kim, H., Gao, J., Tang, J., Hahn, H.T., Chou, T.-W., Itkis, M.E., Haddon, R.C., 2007. Multiscale Carbon Nanotube-Carbon Fiber Reinforcement for Advanced Epoxy Composites. Langmuir 23, 3970-3974.

Brunner, A.J., Blackman, B.R.K., Davies, P., 2008. A status report on delamination resistance testing of polymer-matrix composites. Engineering Fracture Mechanics 75(9), 2779-2794.

Drescher, P., Thomas, M., Borris, J., Riedel, U., Arlt, C. 2013. Strengthening fibre/matrix interphase by fibre surface modification and nanoparticle incorporation into the matrix. Composites Science and Technology 74, 60–66.

Esqué-de los Ojos, D,, Ghisleni, R,, Battisti, A,, Mohanty, G,, Michler, J,, Sort J, Brunner, A.J. 2016. Understanding the mechanical behaviour of fibre/matrix interfaces during push-in tests by means of finite element simulations and a cohesive zone model. Computational Materials Science 117, 330-337.

Ghisleni, R,, Rzepiejewska-Malyska, K,, Philippe, L,, Schwaller, P,, Michler, J. 2009. In situ SEM indentation experiments: instruments, methodology, and applications. Microscopy Research and Technique 72(3), 242–249.

Greisel, M., Jäger, J., Moosburger-Will, J., Sause M.G.R,, Mueller, W.M., Horn S., 2014. Influence of residual thermal stress in carbon fiber-reinforced thermoplastic composites on interfacial fracture toughness evaluated by cyclic single-fiber push-out tests. Composites Part A 66, 117–127.

Herrera-Franco, P.J., Drzal, L.T., 199. Comparison of methods for the measurement of fibre/matrix adhesion in composites. Composites 23(1), 2.27.

Hollaway, L.C., 2010. A review of the present and future utilisation of FRP composites in the civil infra-structure with reference to their important in-service properties Construction and Building Materials 24, 2419–2445.

Jäger, J., Sause, M.G.R., Burkert, F., Moosburger-Will, J., Greisel, M., Horn, S., 2015. Influence of plastic deformation on single-fiber push-out tests of carbon fiber reinforced epoxy resin. Composites Part A 71, 157–167.

Jölly, I., Schlögl, S., Wolfahrt, M., Pinter, G., Fleischmann M, Kern W., 2015. Chemical functionalization of composite surfaces for improved structural bonded repairs. Composites Part B 69, 296–303.

Karger-Kocsis, J., Mahmood, H., Pegoretti, A. 2015. Recent advances in fiber/matrix interphase engineering for polymer composites. Progress in Materials Science 73 (2015) 1–43

Kim, H.S., Oh, E., Hahn, H.T., Lee, K.H., 2015. Enhancement of fracture toughness of hierarchical carbon fiber composites via improved adhesion between carbon nanotubes and carbon fibers. Composites Part A 71, 72–83.

Kinloch, I.A., Suhr, J., Lou, J., Young, R.J., Ajayan, P.M. 2018. Composites with carbon nanotubes and graphene: An outlook. Science 362, 547–553. (2018)

Kumar, A., Sharma, K., Rai Dixit, A., 2020. Carbon nanotube- and graphene-reinforced multiphase polymeric composites: review on their properties and applications. Journal of Materials Science 55, 2682–2724.

McCarthy E.D., Soutis, C., 2019. Determination of interfacial shear strength in continuous fibre composites by multi-fibre fragmentation: A review. Composites Part A 118, 281–292.

Mueller, W.M., Moosburger-Will, J., Sause, M.G.R., Greisel, M., Horn, S. 2015. Quantification of crack area in ceramic matrix composites at single-fiber push-out testing and influence of pyrocarbon fiber coating thickness on interfacial fracture toughness, Journal of the European Ceramic Society 35, 2981–2989.

Mohanty G., Wheeler, J.M., Raghavan, R., Wehrs, I.,, Hasegawa, M.,, Mischler, S., Philippe, L., Michler, J. 2015 Elevated temperature, strain rate jump microcompression of nanocrystalline nickel, Philosophical Magaznie, 95(16-18), 1878-1895.

Rodriguez, M., Molina-Aldareguia, J.M., Gonzalez, C., Llorca, J., 2012 A methodology to measure the inter-face shear strength by means of the fiber push-in test. Composites Science and Technology 72(15), 1924-1932.

Sharma, M., Gao S.L., Mäder, E., Sharma H., Yew Wei L., Bijwe, J. 2014. Carbon fiber surfaces and composite interphases. Composites Science and Technology 102, 35–50.

Stojcevski, F., Timothy B. Hilditch, T.B., Henderson, L.C. 2019. A comparison of interfacial testing methods and sensitivities to carbon fiber surface treatment conditions. Composites Part A 118, 293–301.

Teklal, F., Djebbar, A., Allaoui, S., Hivet, G., Joliff, Y., Kacimi, B. 2018. A review of analytical models to describe pull-out behavior – Fiber/matrix adhesion. Composite Structures 201, 791–815.

Yao, H.W., Sui, X.H., Zhao, Z.B., Xu, Z.W., Chen, L., Deng, H., Liu, Y., Qian, X.M., 2015 Optimization of interfacial microstructure and mechanical properties of carbon fiber/epoxy composites via carbon nanotube sizing. Applied Surface Science 347, 583–590.

Yuan, X.M., Zhu, B., Cai, X., Qiao, K., Zhao, S.Y., Zhang, M. 2019. Nanoscale Toughening of Carbon Fiber-Reinforced Epoxy Composites Through Different Surface Treatments. Polymer Engineering and Science 59(3), 625-632.

Zhang J., Deng, S.Q., Wang, Y.L., Ye, L., Zhou, L.M., Zhang, Z. 2013. Effect of nanoparticles on interfacial properties of carbon fibre–epoxy composites. Composites: Part A 55, 35–44.